CrossMark

RESEARCH PAPER

Hydrophobic patterning of functional porous pigment coatings by inkjet printing

Risto Koivunen[1] · Eveliina Jutila[1] · Roger Bollström[2] · Patrick Gane[1,2]

Abstract Paper-based analytical devices provide novel platforms for functional sensing applications, such as medical diagnostics and environmental monitoring. They are based on porous hydrophilic material, which transports the sample liquid by capillary action. The directional flow of aqueous liquids can be controlled by selective hydrophobising of pores. Earlier research in this field has concentrated on highly porous cellulose papers as base substrates, with no significant interest shown for pigment coatings. Such coatings can produce significantly thinner porous layers, thus requiring smaller sample volumes. This study investigates the hydrophobic patterning of custom-designed porous pigment coatings by functional inkjet printing. Tested coatings consisted of reference ground calcium carbonate and porous functionalised calcium carbonate (FCC) pigments combined with various binders, including microfibrillated cellulose. The hydrophobising custom-made inks contain polystyrene or alkyl ketene dimer (AKD) in *p*-xylene. The patterning is demonstrated by reaction arrays and simple channels. With polystyrene ink, successful hydrophobic barriers could be generated on all tested pigment/binder coatings, although generally requiring printing of multiple layers of barrier material. With AKD ink, hydrophobic patterns could be created successfully on coatings containing an organic binder, but not on coatings with inorganic sodium silicate as binder. The AKD ink generated hydrophobic barriers using fewer ink layers compared with polystyrene ink. Interestingly, AKD ink could hydrophobise the FCC pigment alone without binder, presumably due to hydroxyl groups on the pigment surface. Hydrophobic patterning of the pigment coatings is seen to require large amounts of hydrophobising agent, likely related to the high specific surface area.

Keywords Inkjet printing · Functional printing · Functional coating · Functionalised calcium carbonate · Hydrophobising ink · Paper-based analytical device

Abbreviations
AKD	Alkyl ketene dimer
CMC	Carboxymethyl cellulose
FCC	Functionalised calcium carbonate
GCC	Ground calcium carbonate
MCC	Microcrystalline cellulose
MFC	Microfibrillated cellulose
PP	Polypropylene
PS	Polystyrene
PVOH	Polyvinyl alcohol
SEM	Scanning electron microscopy

1 Introduction and background

Paper-based analytical devices are paper products intended to be used as tools in chemical or medical analysis; pH indicator paper serving as a classic example. Recent research on such analytical devices has introduced the topic of paperfluidics, combining microfluidic concepts with paper or paper-like porous materials. The porous nature allows these devices to absorb and transport liquids within the pore matrix by capillary action.

✉ Risto Koivunen
  risto.koivunen@aalto.fi

[1] Department of Forest Products Technology, School of Chemical Technology, Aalto University, P.O. Box 16300, 00076 Aalto, Finland

[2] Omya International AG, P.O. Box 335, Baslerstrasse 42, 4665 Oftringen, Switzerland

Modern healthcare and environmental monitoring relies on analytical and diagnostic techniques to detect disease and contamination. Sophisticated techniques are available to laboratories and hospitals, but advanced and convenient diagnostic tools are also needed for field, point-of-care and household testing, especially in limited resource settings. Microfluidic diagnostic devices, made easily portable by their small size, and only requiring relatively small sample volumes, may provide practical diagnostic solutions for such settings. However, conventional microfluidic designs, produced by microfabrication technologies, and often requiring external pumping, may be unnecessarily complex for mass-produced applications in the field. By employing commonly available easy-to-process materials, paperfluidic devices may provide an alternative low-cost platform for simple and disposable microfluidic diagnostic tools.

Applications for paperfluidic diagnostic tools include medical assays, such as detection of blood type (Li et al. 2012) or sickle cell disease (Yang et al. 2013) from a small blood sample, monitoring of nitrite levels in saliva for patients undergoing haemodialysis for renal disease (Klasner et al. 2010) or detection of glucose levels in urine (Cassano and Fan 2013). Other possible applications include detection of bacteria in food (Jokerst et al. 2012) or water (Hossain et al. 2012) samples, detection of heavy metals (Feng et al. 2013) or reactive phosphates (Jayawardane et al. 2012) in water, or even detection of explosive traces (Taudte et al. 2013). In the laboratory environment, paperfluidic devices are also expected to provide an economical platform for pharmaceutical research (Chen et al. 2015).

The liquid transport in paperfluidic devices is propelled by capillary pressure in the hydrophilic pore matrix, in which hydrophobic barriers are employed to limit and direct the flow. These barriers are fabricated by treating the pore surfaces on selected areas of the substrate with hydrophobic material, resulting in a surface chemistry that no longer facilitates capillary transport of high surface tension aqueous samples. Microfabrication methods, such as photolithography (Martinez et al. 2007), and various printing methods provide the means for patterning such barriers. The most common method of printing hydrophobic patterns on laboratory scale has been inkjet, depositing a variety of hydrophobic materials, such as hot melt wax (Carrilho et al. 2009a), solvent-diluted polydimethylsiloxane (Määttänen et al. 2011), UV-curing polymer (Maejima et al. 2013) and acrylic polymer in solvent-based solution (Apilux et al. 2013). The two key properties of a hydrophobising printing ink comprise the ability to penetrate the full depth of the porous part of the substrate and the ability to transform pore surface chemistry from hydrophilic into hydrophobic.

On the simplest level, a paper-based analytical device may consist of a single reaction test zone, limited by hydrophobic barriers. A paper-based equivalent to the injection-moulded microzone well-plate can be manufactured by printing an array of such patterns on a sheet, with assays conducted in the test zones being measurable with spectrophotometric techniques based on absorbance, reflectance or fluorescence (Carrilho et al. 2009b). Printing electrodes on test zones enable electrochemical (Määttänen et al. 2013) and electrochemiluminescent (Delaney et al. 2011) detection. More complex paperfluidic devices may feature separate areas for sample insertion, reaction and detection, connected to each other with channels.

To date, most studies on paperfluidic devices have been conducted with highly porous cellulose papers, including commercial chromatography (Martinez et al. 2007) or filter (Li et al. 2010) papers and custom laboratory handsheets (Böhm et al. 2014), as base substrates. Another studied substrate is nitrocellulose membrane (Lu et al. 2010b; Apilux et al. 2013), employed currently in commercial lateral flow tests. Porous cellulose papers benefit from being easily available, disposable, naturally wicking and white in colour. However, due to the dimensions of the fibres, typically 10–20 μm wide (Evans et al. 2014), such papers tend to lack uniformity on the local micro- and even macroscale. This lack of uniformity within a sheet is further complicated by the fibre orientation inherent to industrial paper manufacturing, resulting in paper having different mechanical properties in machine and cross-machine directions (Pelton 2009). Typically employed filter and chromatography papers are not designed with printing applications in mind, and display low tensile wet strength, as well as high surface roughness and uneven pore size distribution, which makes them very challenging substrates even for flexographic printing (Koivula et al. 2013). Certain bioagents, such as proteins, do not bind well to native cellulose without additional surface chemistry modification (Pelton 2009). Patterned cellulosic paper is also open on both sides, thus risking contamination from any surface it is placed on. The paper can be protected with a polymer film attached with adhesive (Fenton et al. 2009) or hot lamination (Cassano and Fan 2013), but these methods have limitations: adhesives can leach into the paper or samples, while hot lamination alters the pore matrix structure, resulting in reduced wicking speed. Alternatively, one side of the paper can be printed with a limited layer of hydrophobising material (Zhong et al. 2012), though in such case there is a risk of the material penetrating too deeply or unevenly to the paper.

In contrast to cellulosic papers, pigment paper coatings as alternative base substrates have received little interest, since typical paper coatings designed for traditional offset printing do not exhibit the necessary volume capacity and permeability in their capillary pore structure. Furthermore, there has been a lack of clear design requirements proposed
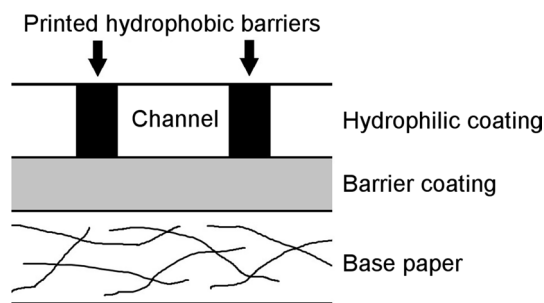
Fig. 1 Schematic cross section of multi-layer coated paper with printed hydrophobic pattern: not to scale

for speciality coatings for diagnostic applications. Pigment coatings consist of fine micrometre-sized pigment particles, usually mineral, and binders, which tie the particles to each other and to the base substrate, with connected voids between particles forming a pore network. Due to the finer particle size and manufacturing methods employed, they tend to form significantly more uniform pore matrices than cellulose fibre-based paper. While commercially available coated papers are not designed for paperfluidic applications, they can still be hydrophobically patterned to form reaction arrays (Määttänen et al. 2011). Custom-designed multi-layer coated papers, consisting of base paper, isolating barrier pre-coating layer (Bollström et al. 2013) and custom hydrophilic top coating, as demonstrated in Fig. 1, can provide platforms for mass-produced paperfluidic devices.

This study is part of the early phase of a larger research project investigating the possibilities of employing novel specially designed pigment coatings as generic base substrates for mass-fabricated printed paperfluidic devices, with potential applications ranging from new laboratory research tools to point-of-care diagnostics. Such coated substrate designs provide numerous advantages compared with plain cellulose paper. Firstly, the pigment particles feature spatial dimensions smaller than those of cellulose fibres, providing a better printing resolution and colour reproduction with graphic inks and potentially also better resolution with functional inks. The particle dimensions also result in finer pore dimensions, leading to more effective filtering of small particles and the potential for molecular selection. Secondly, the thickness of the functional coating layer can be varied freely, enabling the production of very thin wicking layers requiring minimal liquid sample and reagent volumes. Minimal sample requirements are likely to be important when assays are taken from patients in cases where access to or available volumes are strictly limited. One example is lacrimal fluid on the eye, especially from patients suffering from dry eye syndrome (Kim and Noh 2013). Additionally, small reagent volumes reduce

material expenses and possibly manufacturing times, particularly if inkjet printing is used for applying the reagents. On thick substrates, optical analysis depth is limited since the bulk of the substrate limits the amount of light that can penetrate deep into the substrate and return to the surface (Yetisen et al. 2013). Thirdly, when a barrier layer or an impermeable base substrate is employed, the underside of the hydrophilic layer is isolated from the environment, hence allowing the device to be placed on a surface while containing liquid. Furthermore, the base paper is isolated from liquids in the top coating by the barrier layer. Fourthly, pigments provide novel surface chemistry, expected to help with immobilisation of reagents or separation of components from the liquid sample by the various mechanisms of chromatography.

The functional coatings employed in this study consist of a porous functionalised calcium carbonate (FCC) pigment, derived from a modification of calcium carbonate, combined with a variety of organic and inorganic binders. The FCC pigment was used in previous studies by the current authors to illustrate the high level of capillarity achievable (Jutila et al. 2015). In the present work, hydrophobic barriers are applied to coatings featuring a variety of binders, including polymer latex, inorganic sodium silicate, polyvinyl hydroxide, carboxymethyl cellulose and microfibrillated and microcrystalline cellulose (MFC, MCC). To simplify the testing procedures, impermeable base substrates are used in this work to provide support for the pigment coatings. Permeable filter paper substrate is used as a reference.

Biosensor applications involve addition of bioagents, such as enzymes or antibodies, on the sensor substrate. Such bioagents should remain immobilised and active on the substrate for extended periods of time. On paper-based devices, storage stability of enzymes has been improved by binding them within mesoporous silica nanorods before depositing them on filter paper (Zhao et al. 2013) or by sandwiching them between layers of porous silica sol–gel applied on coated cardboard (Hossain et al. 2009) or filter paper (Koivula et al. 2013). Commercial ground calcium carbonate, commonly employed as paper filler or coating pigment, is not a good platform for enzyme immobilisation, as demonstrated by the poor adsorption and binding of horseradish peroxidase, for example, resulting from the presence of dispersing agents (Di Risio and Yan 2010). The situation can be improved of course by omitting, limiting or changing the typical anionic dispersing agents used.

Unlike typical coating pigments, such as kaolin or ground calcium carbonate, the surfaces of FCC particles, employed in this study, contain no surface additives and consist mainly of nanoporous hydroxylapatite, a major component of human bones, which is expected to provide both large surface area and a suitable surface chemistry for

Table 1 Pigment properties

Pigment	Specific surface area (m^2 g^{-1})	Calcium carbonate content (w/w%)	Hydroxylapatite content (w/w%)	Other mineral content (w/w%)
GCC12	12.5	98.3	0.0	1.7
FCC40	40.0	74.5	25.5	0.0
FCC105	105.0	15.2	84.8	0.0

binding bioagents. On electrode-based biosensors, hydroxylapatite-based materials have been applied to immobilise and stabilise bioagents, including glucose oxidase (Zhang et al. 2009) and horseradish peroxidase enzyme (Li et al. 2011) on plain hydroxylapatite, as well as transferrin antibodies (Yang et al. 2005) and tyrosinase enzyme (Lu et al. 2010a) on hydroxylapatite–chitosan composite materials. However, these studies were carried out with sensors typically stored in buffer solution, rather than in the dry state. In medical applications, hydroxylapatite–alginate microspheres have been demonstrated as carriers for glucocerebrosidase enzyme (Ribeiro et al. 2004).

The specific topic of the present study is on investigating the hydrophobic patterning of these above-mentioned novel coated substrates. This is carried out by inkjet printing of custom functional inks consisting of polystyrene (PS), or the paper sizing agent alkyl ketene dimer (AKD), dissolved in organic solvent. These inks have been shown to be effective for hydrophobic patterning of filter papers (Koivunen et al. 2015). AKD-based inkjet inks have been applied to hydrophobic patterning also by other authors, either dissolved in organic solvent (Li et al. 2010) or as an aqueous emulsion (Wang et al. 2014), while PS-based inks have been printed with flexography (Olkkonen et al. 2011) and screen printing (Sameenoi et al. 2014). This study emphasises print settings required for the successful hydrophobisation of the custom pigment coatings, as well as demonstrating various methods for testing the resulting hydrophobic patterning.

2 Materials and methods

2.1 Functional pigment coatings

The three different pigments tested were commercial ground calcium carbonate Hydrocarb® 90 ME (polyacrylate-dispersed marble-based product with 90 w/w% of particles finer than 2 μm), from here on referred to as GCC12, and two versions of an experimental highly porous form of modified calcium carbonate in pure form, known as functionalised calcium carbonate (FCC), with the two versions from here on referred to as FCC40 and FCC105. All the pigments were provided by Omya International AG (Oftringen, Switzerland). Data on pigment properties, as

provided by the manufacturer, are listed in Table 1, with mineral content distribution determined by X-ray diffraction (XRD) analysis and specific surface area (m^{2}g^{-1}) by the nitrogen adsorption method (BET) (Brunauer et al. 1938). Pigment abbreviations (GCC12, FCC40, FCC105) are derived from a combination of pigment type/content and specific surface area.

FCC differs from plain calcium carbonate pigment by having a microporous-reconstructed surface containing hydroxylapatite ($Ca_5(PO_4)_3OH$), resulting in highly hydrophilic particles with large surface area and surface hydroxyl groups. Figure 2 displays scanning electron microscope (SEM) images of FCC105 pigment particles, with and without binder.

Seven different binders were tested with the pigments, namely:

1. Microfibrillated cellulose (MFC A) Arbocel MF-40-7 (J. Rettenmaier & Söhne GmbH + Co KG, Rosenberg, Germany).
2. Microfibrillated cellulose (MFC B), mechanically produced, 22.3462 CMCX-TYPE (Omya International AG, Oftringen, Switzerland).
3. Microcrystalline cellulose (MCC) Vivapur 105 (J. Rettenmaier & Söhne GmbH + Co KG, Rosenberg, Germany).
4. Carboxymethyl cellulose (CMC) Finnfix 5 (CP Kelco, Äänekoski, Finland).
5. Polyvinyl alcohol (PVOH) BF05 (Omya International AG, Oftringen, Switzerland).
6. Styrene acrylic latex Acronal S 728 (BASF, Ludwigshafen, Germany).
7. Sodium silicate (Merck KGaA, Darmstadt, Germany, product number 1056212500).

Each coating colour consisted of a single pigment, a single binder and water, with solid content varied to produce a suspension with viscosity suitable for coating. No additives, such as dispersing agents, were included in the formulations. FCC105 pigment, being the main interest of this study due to its high surface area, was tested first with each of the binders, as well as without any binder. Based on the initial results obtained with the FCC105 coatings, microfibrillated cellulose (MFC A) was then chosen as the binder for the additional coatings containing FCC40 and GCC12
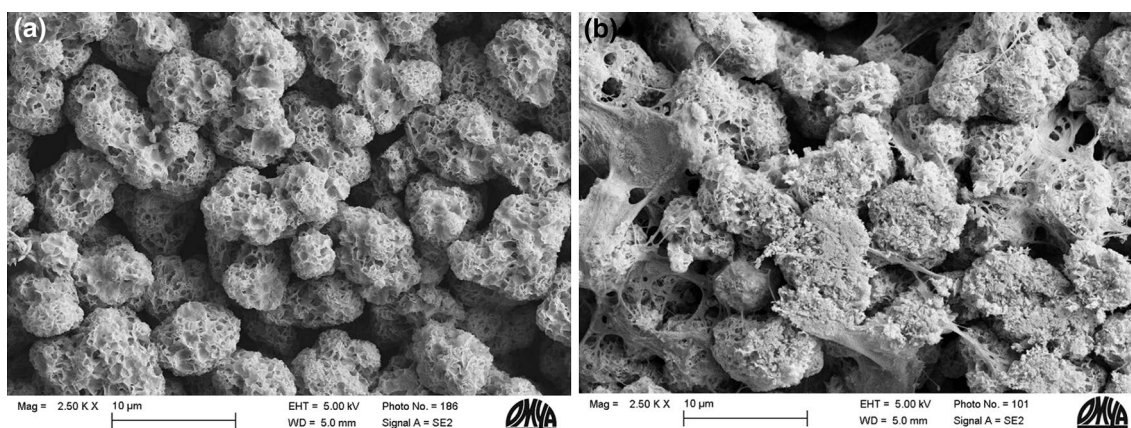
Fig. 2 Scanning electron microscope images of FCC105 particles: **a** plain and **b** combined with Arbocel MF-40-7 microfibrillated cellulose as binder

Table 2 Coating colour formulations

Name	Pigment	Binder	Nominal binder amount (pph)[a]	Solids content (w/w%)
GCC12 + MFC A	GCC12	Microfibrillated cellulose Arbocel MF-40-7	20	27.7
FCC40 + MFC A	FCC40	Microfibrillated cellulose Arbocel MF-40-7	20	17.4
FCC105 + MFC A	FCC105	Microfibrillated cellulose Arbocel MF-40-7	20	14.9
FCC105 + MFC B	FCC105	Microfibrillated cellulose 22.3462 CMCX-TYPE	20	4.4
FCC105 + MCC	FCC105	Microcrystalline cellulose Vivapur 105	20	13.7
FCC105 + CMC	FCC105	Carboxymethyl cellulose Finnfix 5	10	14.3
FCC105 + PVOH	FCC105	Polyvinyl alcohol BF05	10	14.3
FCC105 + latex	FCC105	Styrene acrylic latex Acronal S 728	10	10.0
FCC105 + sodium silicate	FCC105	Sodium silicate	50	19.2
FCC105	FCC105	–	0	14.4

[a] pph for binder stands for parts by weight per 100 parts by weight of pigment

pigment. Table 2 lists all the coating colour formulations, and they will be from here on referred to by the names given in Table 2.

Coating colours were applied with a mechanical drawdown K202 Control Coater (RK PrintCoat Instruments Ltd., Herts, UK) with blue labelled wire-wound rod, applying a 100-μm-thick wet film onto the substrate, with a speed setting of 6 m min^{-1}. Other available rods for this coater cover various film thicknesses between 4 and 500 μm. Coated substrates were allowed to dry at room temperature overnight.

The coatings were applied on three different types of base substrate. FCC105 coating, lacking any binder, could be safely handled only when on a rigid surface and was therefore applied to 25 × 75 and 100 × 200 mm^2 glass slides. All other coating colours were applied on two flexible substrates, these being 180 × 260 mm^2 sheets of impermeable pigment-filled polypropylene (PP) film

SuperYUPO® (Yupo Corporation, Tokyo, Japan), previously also known as Synteape, of 80-μm thickness and 62 g m^{-2} basis weight, and aluminium foil. Unless explicitly mentioned otherwise, any future results are given for the coatings applied on the PP film.

2.2 Functional inks

Hydrophobic inks were prepared by dissolving 5.0 w/w% of hydrophobising agent and 0.1 w/w% of colourant in p-xylene solvent (VWR, Vienna, Austria, product code 28984.292). The ink components were allowed to dissolve overnight without external agitation. Before use, the inks were filtered with 0.45-μm GHP Acrodisc GF syringe filters (Pall Corporation, Port Washington, USA).

Two different hydrophobising agents were applied, these being 35-kDa molecular weight polystyrene (Sigma-Aldrich, St. Louis, USA, product code 331651) and solid

Fig. 3 Graphic visualisation of custom waveform shapes, displaying **a** jetting segments for AKD ink, **b** non-jetting segments for AKD ink, **c** jetting segments for PS ink and **d** non-jetting segments for PS ink, all as visualised by the waveform editor for the printer
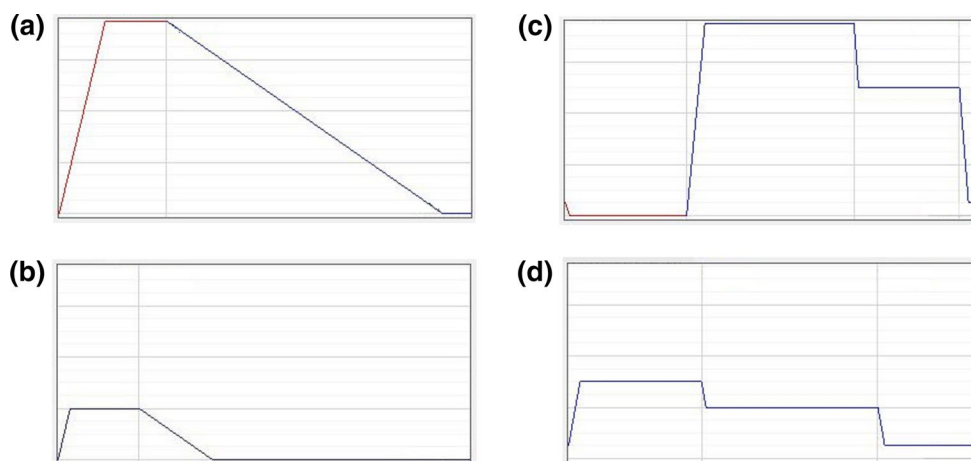
alkyl ketene dimer (AKD) Basoplast 88 (BASF, Ludwig-shafen, Germany). AKD is conventionally used in paper industry for internal sizing (hydrophobising) of paper through reaction with cellulose. From here on, the ink with polystyrene as hydrophobising agent will be referred to as PS ink, while the ink with alkyl ketene dimer will be referred to as AKD ink.

To identify the position and print quality resolution, three different colourants were applied in the ink formulation, these being Sudan Red G (Sigma-Aldrich, St. Louis, USA, product code 17373), yellow dye, wood stain colourant 157 (Kremer Pigmente GmbH & Co. KG, Aichstetten, Germany, product number 94010) and Blue 807 dye (Kremer Pigmente GmbH, & Co. KG, Aichstetten, Germany, product number 94030). PS ink was coloured only with Sudan Red G, while AKD inks were prepared separately with each colourant. Unless otherwise mentioned, references to AKD ink are to the version coloured with Sudan Red G.

Inks were printed with a DMP-2831 research inkjet printer (Fujifilm Dimatix, Santa Clara, CA, USA) employing DMC-11610 ink cartridges with 10 pl nominal drop volume. For both inks, the printer mounting platen and print head were heated to 30 °C, and printing was performed with all 16 available nozzles, with print head nozzle meniscus vacuum set to 4.0 in. (10.16 cm) H_2O. Custom print head waveforms for the inks, shown in Fig. 3 and listed in Table 3, were experimentally designed to provide satisfactory and reliable drop formation. The waveform parameters level, slew and duration refer to the %-age amplitude of the voltage applied to bend the fluid chamber membrane, the slew rate controlling how fast the membrane is being bent, and time consumed to bend and keep the membrane in position, respectively.

PS ink was observed to become non-jetting at nozzles left idle for some time, presumably due to viscous build-up as a result of concentration. To counter this, a cleaning

Table 3 Custom waveforms for PS and AKD inks

Ink	Segment	Level (%)	Slew	Duration (μs)
PS	Jetting 1	0	0.65	3.392
	Jetting 2	100	2.00	4.672
	Jetting 3	67	2.00	2.944
	Jetting 4	7	2.00	0.512
	Non-jetting 1	40	1.00	3.712
	Non-jetting 2	27	1.00	4.928
	Non-jetting 3	7	1.00	2.880
AKD	Jetting 1	100	0.30	7.488
	Jetting 2	0	0.05	21.248
	Non-jetting 1	27	0.30	5.632
	Non-jetting 2	0	0.05	23.104

cycle, consisting of a 0.1-s purge operation adopting external overpressure applied to force ink out of nozzles, was run automatically at the beginning of the printing operation and at 5-min intervals during the printing. With AKD ink, no such similar problem was observed, and instead a manufacturer provided *Spit Spit* cleaning cycle, applying only the regular jetting mechanism, was applied to prime the nozzles automatically at the beginning of the printing operation and at 10-min intervals during the printing. The same cleaning cycle was also run at the end of printing for both inks.

Drop spacing and number of ink layers were used as parameters to adjust the amount of ink applied per unit area of substrate. After printing, the samples were allowed to stand for approximately 1 min to allow solvent to evaporate. Samples printed with PS ink were ready to use after this short period, while samples printed with AKD ink were heat treated for 10 min either on a 100 °C hot plate or in a 105 °C oven to ensure that AKD could react with hydroxyl groups present in the coating. The PP films shrank slightly in one dimension as a result of this heat treatment, losing

roughly 1 % of their original width of 180 mm. Furthermore, Sudan Red G colourant was seen to smear on heat treatment, making it difficult to assess optically the exact edge of the printed pattern. Therefore, AKD ink coloured with Blue 807 Dye was chosen for printing samples requiring such assessment.

Printed samples were mainly stored inside plastic sleeves and protected from light. Under these conditions, both Sudan Red G and Blue 807 Dye seemed to remain stable on the coatings. However, some samples were stored in the open in a well-ventilated area, and under these specific conditions both Sudan Red G and Blue 807 Dye displayed major fading after a few months. Printed samples coloured with yellow dye, wood stain colourant 157, were all consumed during the analysis process, and thus, the stability of this colourant over time on the coatings could not be recorded.

2.3 Other materials

Wicking speed and/or integrity of the hydrophobic patterns was tested with a variety of aqueous solutions. Firstly, deionised water was applied plain or dyed with 0.1 w/w% of Amaranth red (Fluka Chemie AG, Buchs, Switzerland, product code 06409) or rhodamine B (Kremer Pigmente GmbH & Co. KG, Aichstetten, Germany, product number 94900). Secondly, aqueous solutions containing 15, 20, 25, 30 or 40 w/w% ethanol and 0.1 w/w% rhodamine B were prepared for application as low surface tension liquids to test hydrophobic barrier resistance to penetration. Thirdly, aqueous non-ionic surfactant solutions, containing 1.0 w/w% Tween 80 (Sigma-Aldrich, St. Louis, USA, product code 1754) in aqueous solution, both undyed and with 0.1 % by weight rhodamine B, were prepared.

Whatman 4 cellulose filter paper (GE Healthcare UK Ltd., Little Chalfont, UK) acted as a reference substrate, in order to demonstrate the differences between conventional paperfluidic material and the custom-designed coatings. According to the manufacturer, this filter paper has particle retention of 20–25 μm.

2.4 Pigment coating characterisation methods

Coating dry thickness was measured with an SE250D micrometer (Lorentzen & Wettre, Kista, Sweden) with a 2 cm^2 measurement area spindle and measurement pressure of 100 kPa. Thickness was measured from coated PP films, with the actual coating thickness considered to be equal to the measured thickness minus 80 μm (nominal thickness for the PP films in this study). Ten measurements were taken per coating.

Cumulative coating pore volume was measured as a function of mercury intrusion pressure with an Autopore IV porosimeter (Micromeritics, Norcross, GA, USA) from coatings applied on aluminium foil, with a single sample measured per coating. Scanning electron microscopy (SEM) micrographs were obtained with a Sigma VP field emission scanning electron microscope (Carl Zeiss AG, Oberkochen, Germany).

Wicking speed was measured from cut 3×75 mm^2 strips of coating applied on PP film, attached with double-sided tape to 25×75 mm^2 glass slides to provide stiffness. These slides were then placed vertically into an open cylindrical plastic jar (33 mm inner diameter, 68 mm high), with 4 mm of rhodamine B-dyed water at the bottom of the jar. Liquid was allowed to wick along the coating for 5 min in controlled climate (21 °C, 65 % RH), after which the sample was removed from the jar, and the distance travelled by the water was measured with a scale rule. Three samples were measured per coating. Exceptions to the standard set-up were made for the FCC105 coating and Whatman 4 filter paper. FCC105 coating was measured from directly coated 25×75 mm^2 glass slides. Whatman 4 filter paper strips, cut to the 3×75 mm^2 size, were attached to glass slides only from one end, with the slide then placed on top of the jar so that the filter paper strip was freely hanging from it at right angles. The purpose of this method was to avoid any additional capillary effect that could take place between the porous paper and the glass slide.

2.5 Functional ink and aqueous test solution characterisation methods

The surface tension of inks, as well as ethanol or surfactant containing test solutions, was measured with a CAM200 contact angle measurement system (KSV, Espoo, Finland) by the pendant drop method in a laboratory room maintained at 22 °C. Drops were formed with an integral dispenser using LH-L7902000 low-retention pipette tips (Sartorius Biohit Liquid Handling Oy, Helsinki, Finland). For each liquid, ten drops were tested, with each drop being measured ten times in succession at 1-s intervals.

The liquid contact angle between select test liquids and native or printed coatings was evaluated with the same CAM200 system by applying a 1-μl (ethanol or surfactant solution) or a 4-μl (deionised water) drop on the substrate. The contact angle was then measured at 1-s intervals for a time period of 1–30 s from the application of the drop. For each tested substrate and test solution combination, five drops were measured.

Ink viscosity was determined with an MCR-300 rheometer (Paar Physica, Graz, Austria) with a PP50 flat disc spindle and a P-PTD 150 Peltier base plate. Viscosity measurements were taken at a shear rate of 100 s^{-1} at 30 °C. Three samples per ink were measured, with each sample measured ten times in succession at 30-s intervals.

Fig. 4 An example of the ring test pattern, printed with PS ink on FCC105 + MFC B-coated substrate, with drop spacing of 20 µm and 1, 2, 3 and 4 ink layers, respectively
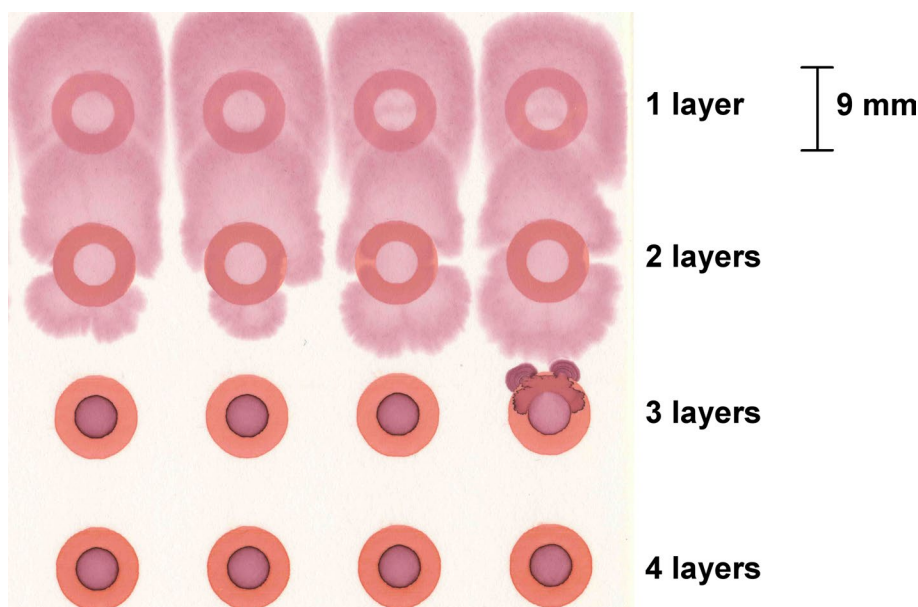
Ink drop mass was measured by jetting samples consisting of 20 million drops on pre-weighed aluminium pans, waiting overnight to ensure that all solvent had evaporated and reweighing the pans to determine the dry solids weights, from which the original sample mass in each case could then be calculated. Ten samples were tested per ink.

2.6 Hydrophobic test patterns

The amount of hydrophobic ink per unit area required to produce effective and reliable barriers on the substrates was determined with a ring test pattern, consisting of a series of rings with nominal 5 mm inner and 9 mm outer diameters. Ring test patterns were printed on the substrates with drop spacing values of 10, 15 and 20 µm, with the printed rings containing 638 730, 193 352 and 110 716 printed pixels (drops) per ring, respectively. For comparison, the print head nozzle diameter is 21.5 µm. Effect of multiple ink layers, printed on top of each other after the previous layer had dried, was investigated by printing up to 5 layers for the PS ink and 2 layers for the AKD ink. Ten rings, printed in parallel, were tested for each studied combination of coating, ink, drop spacing and number of ink layers. As an exception, FCC105 coating applied on glass was only tested with 8 rings, due to the smaller coated area on the plate limiting the number of rings that could be printed in parallel.

Barrier properties of the rings were tested by pipetting a 10-µl drop of Amaranth red-dyed water on the centre of each ring and allowing the drop to dry. Tests were conducted at 21–23 °C and 50–65 % RH. Figure 4 shows an example of the ring test pattern after testing. Tested print settings were considered to provide reliable hydrophobisation if all 10 tested rings contained the test liquid fully within the interior of the ring, while any leaking is considered to disqualify the tested settings, with leakage defined as any spreading of the colourant in the sample beyond the inner boundary of the ring. It should be noted that the 10-µl drop has significantly higher volume than can be absorbed by the coating within the ring, and thus possible spreading of liquid beyond the ring can be by capillary transport, surface spreading or combination of both. Thus, to be successful, the ring test barrier has to stop both surface spreading and capillary wicking.

The minimum functional hydrophobic barrier width was evaluated by considering the blocking of purely capillary transport using a separate previously demonstrated barrier test pattern (Koivunen et al. 2015), consisting of 10 parallel channels with barriers of 0.1–1.0 mm in nominal width printed across their entrances, plus 1 control channel with no barrier. For testing, patterns were cut off and placed vertically in cylindrical jars (52 mm inner diameter, 65 mm high) with approximately 4 mm of rhodamine B-dyed water placed in the bottom. Jars were closed to restrict evaporation. After 60 min, the barriers were visually assessed to determine which ones had been wicked through and which ones had successfully contained the water from entering the channel. The narrowest barrier to contain water on a group of 10 identical test samples was defined as the minimum reliable barrier width, with the actual width of this barrier determined by image analysis of patterns scanned before the test was conducted. Figure 5a–c displays the barrier test patterns.

To test the functional print resolution achievable, a series of decreasing channel widths were evaluated in respect of uninterrupted capillary transport. A channel pattern was printed consisting of 16 parallel test channels (plus seventeenth channel as end filler), each separated by barriers of 1 mm nominal width. The flow channels varied in

Fig. 5 Examples of test patterns. Barriers: **a** schematic, **b** printed, **c** after testing. Channels: **d** schematic, **e** printed, **f** after testing
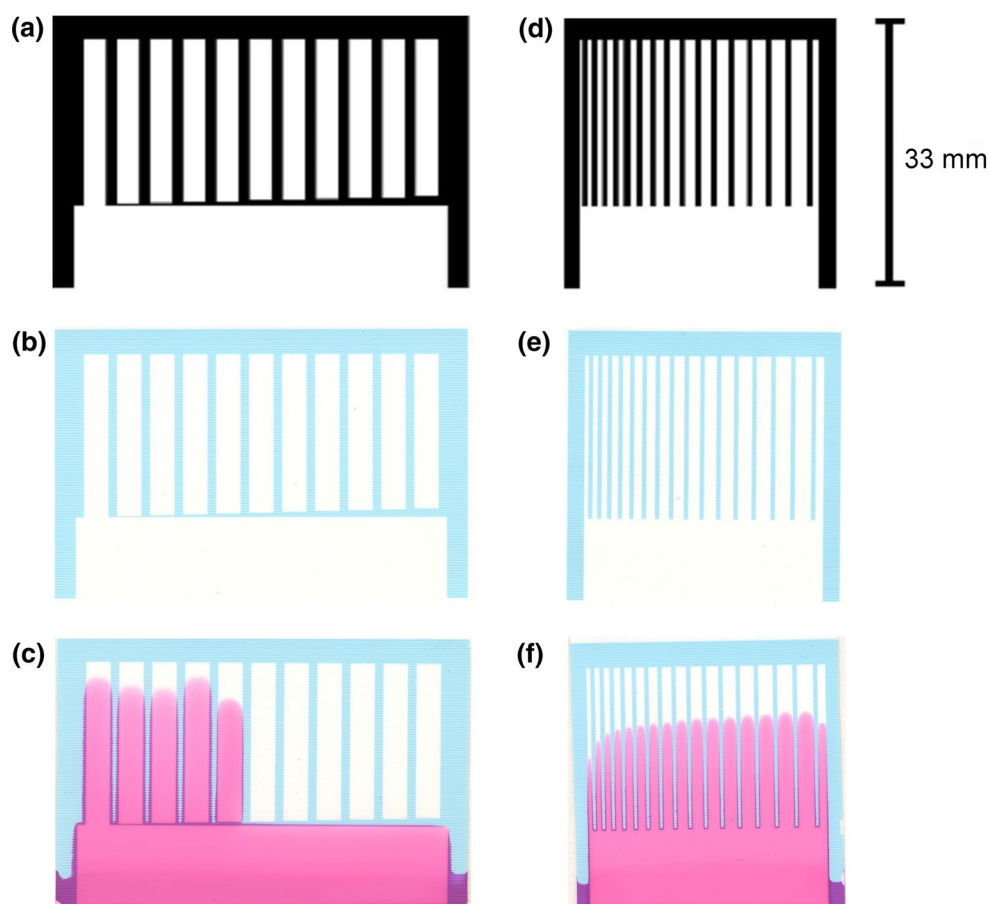
33 mm

nominal width from 0.5 to 2.0 mm in 0.1-mm intervals. To determine in which channels liquid freely flows the whole length of the channel, printed test patterns were placed vertically in open cylindrical plastic jars (33 mm inner diameter, 68 mm high) with approximately 4 mm of rhodamine B-dyed water in its base. After 10 min, the samples were observed to determine the narrowest channel where water had reached the top. The narrowest channel where water reached the top on a group of 10 identical test samples was defined as the minimum reliable channel width, with the actual width of this channel determined by image analysis of patterns scanned before the test was conducted. Figure 5d–f illustrates channel width test patterns.

Ink spreading on the coatings was measured by printing a line spreading pattern consisting of ten parallel lines, ranging in nominal width from 0.1 to 1.0 mm. Furthermore, ink spreading was also analysed from the printed ring test patterns.

Printed patterns were scanned with an Epson Expression 1680 flatbed scanner (Seiko Epson Corporation, Nagano, Japan), and the scanned patterns analysed with ImageJ 1.47v image analysis software (National Institutes of Health, Bethesda, MD, USA). Scanning was conducted at 1200 dpi (ring test patterns) or 3200 dpi (barrier, channel and line spreading test patterns) resolution.

3 Results and discussion

3.1 Coating and filter paper properties

Measured coating properties, together with those of the reference filter paper, are listed in Table 4. Specific pore volume is divided into intra-particle pore volume (found within the nanopores situated inside the pigment particles), inter-particle volume (the volume present between the particles in the coating compact) and combined pore volume (intra-particle + inter-particle volume). It is important to note that no deconvolution between the two regions is made in the case where they overlap, but rather a simple cut-off at the intersection point is applied. Cut-off diameter d^* indicates, therefore, the pore diameter at which the split between intra- and inter-particle regions occurs, while a second cut-off diameter d^{**} indicates the upper measurement limit of the inter-particle region. Porosity has been calculated from basis weight, thickness and combined specific pore volume.

Surface strength and adhesion of the coatings were not formally studied, but in general the binder-containing coatings could be handled without coating disintegrating or coming detached from the base substrate. However, writing

Table 4 Measured substrate properties for coatings and filter paper

Substrate	Basis weight (dry) (gm⁻²)	Thickness (dry) (μm)	Wicking distance (in 5 min) (mm)	Intra-particle specific pore volume (cm³g⁻¹)	Inter-particle specific pore volume (cm³g⁻¹)	Combined specific pore volume (cm³g⁻¹)	$d*$ (μm)	$d**$ (μm)	Combined pore volume per unit area (cm³m⁻²)	Porosity
GCC12 + MFC A	32.0 ± 1.4	23 ± 2	2 ± 1	0.00	0.10	0.10	0.57	0.8	3.2 ± 0.1	0.14
FCC40 + MFC A	19.8 ± 2.9	58 ± 2	16 ± 1	0.13	0.18	0.30	0.18	1.8	5.9 ± 0.9	0.10
FCC105 + MFC A	14.0 ± 2.4	62 ± 2	31 ± 1	0.46	0.59	1.05	0.64	7.8	14.7 ± 2.5	0.24
FCC105 + MFC B	4.1 ± 1.4	27 ± 2	23 ± 1	1.24	1.56	2.80	0.79	9.3	11.5 ± 3.9	0.43
FCC105 + MCC	17.1 ± 1.8	73 ± 10	25 ± 6	1.50	2.38	3.88	0.65	9.3	66.3 ± 7.0	0.91
FCC105 + CMC	16.5 ± 2.6	65 ± 2	21 ± 1	1.27	1.69	2.96	0.8	9.3	48.8 ± 7.7	0.75
FCC105 + PVOH	17.9 ± 0.8	70 ± 2	21 ± 1	0.82	1.16	1.98	0.8	9.3	35.4 ± 1.6	0.51
FCC105 + latex	11.8 ± 0.5	60 ± 2	12 ± 2	1.07	1.80	2.87	0.8	9.3	33.9 ± 1.4	0.56
FCC105 + sodium silicate	22.2 ± 1.7	76 ± 6	32 ± 1	0.82	1.27	2.08	0.8	9.3	46.2 ± 3.5	0.61
FCC105	18.8 ± 3.1	–	41 ± 4	–	–	–	–	–	–	–
Whatman 4	92.2 ± 2.2	210 ± 8	57 ± 4	0	1.23	1.23	0	–	113.4 ± 2.7	0.54

Dash (–) indicates that the property in question could not be measured for the given substrate. Values are given with 95 % confidence intervals where available

on a coating with fine pencil generally resulted in coating coming loose in most cases, with the specific exceptions of GCC12 + MFC A and FCC105 + MFC B. Since the samples were printed with inkjet, a non-contact method, they did not come into contact with any moving parts during the printing, and so surface strength was not critical in this study. One of the coatings, FCC105 + MCC, had very poor adhesion and could be removed from the base substrate very easily, making this coating difficult to measure and possibly creating measurement errors.

As regards thickness, most of the coatings are in a similar range (58–76 μm average thickness). However, two coatings are significantly thinner, being under 30 μm thick. Out of these, the GCC12 + MFC A coating has very low specific pore volume, while FCC105 + MFC B coating is highly porous but was coated from a slurry with very low solid content (4.4 w/w%) without any added dispersant. For FCC105 coating with no binder, the thickness could not be reliably measured, since the poor adhesion resulted in some of the coating breaking off during the measurement and then adhering to the measurement spindle platen. Also due to poor adhesion, this pigment could not be applied to aluminium foil for porosity measurements. It would have been possible to measure pore volumes from a pressed tablet instead, but this was not pursued due to the wish to maintain equivalent sample preparation conditions.

Wicking speed was recorded visually using rhodamine B solution. In all coatings, there was slight separation between the colourant and water, due to a chromatographic effect depleting the colourant at the wetting front, so the wicking distance had to be measured eventually from the less visible water front that was a few mm ahead of the very easily visible colourant front. As can be seen from the results, Whatman 4 filter paper had faster wicking speed than any of the coatings. The pure FCC105 coating without any binder had the fastest wicking speed among the set of coatings, while addition of binders to FCC105 resulted in coatings with a variety of wicking speeds: styrene acrylic latex, common in commercial paper coatings, resulted in the slowest wicking speed, while MFC A binder resulted in the fastest wicking speed. However, this property of MFC A to produce highly wicking coatings is not independent of the pigment: combining it with low surface area FCC40 resulted in a more slowly wicking coating and combining it with GCC12 resulted in an almost totally non-wicking coating. FCC pigment with higher specific surface area than those presented in this study could be expected to produce higher wicking speeds and thus bring the coatings closer to filter paper in this aspect. Practical paperfluidic applications require that liquid traverses the channels within a reasonable time, thus wicking speed sets a limit for the maximum practical dimensions of a device.

The results above suggest that designing a fast wicking coating requires an optimal combination of both pigment and binder, where the hydrophilicity of the binder and its distribution amongst pores, affecting primarily pore connectivity, are crucial factors. It is known that certain hydrophilic binders present in the coating, such as polyvinyl alcohol (PVOH) (Lamminmäki et al. 2009) undergo swelling when exposed to water, resulting in dynamic reduction in pore radii as water wicks along the coating. Amongst the binders present in this study, also the various cellulose-based binders (CMC, MCC, MFC) are likely to exhibit such swelling or even solubility in some cases. Nonetheless, it can be concluded that effecting different combinations of pigment and binder will result in different wicking speeds, additionally also affected by the amount of binder present. It should, thus, be possible to engineer new speciality coatings with very specific wicking speeds and functional material interactions.

3.2 Functional ink properties

Table 5 lists the measured physical characteristics and selected print settings for the studied inks. Jetting frequency and voltage were selected so as to give satisfactory drop formation and reliable print performance with the chosen waveforms. Jetting speed was estimated with the integral drop monitoring camera of the DMP-2831 printer.

Values for the AKD ink are given for the version dyed with Sudan Red G, used for printing most of the test patterns. AKD inks dyed with the other two colourants were not explicitly measured, though they are assumed to be very similar since they resulted in similar jetting performance with the same print settings.

Table 5 Ink characteristics: values given with 95 % confidence intervals where available

Ink	PS ink	AKD ink
Viscosity (mPa s)	1.27 ± 0.04	0.62 ± 0.03
Surface tension (mN m^{-1})	27.8 ± 0.1	28.1 ± 0.3
Drop mass (ng)	8.0 ± 1.1	8.3 ± 0.6
Jetting frequency (kHz)	6.0	2.0
Jetting voltage (V)	18.0	17.0
Jetting speed (m s^{-1})	6	5

Regarding viscosity, it is worth keeping in mind that the used shear rate of 100 s^{-1} is not representative of the high shear rates, typically from 10^5 to 10^6 s^{-1}, present within the piezoelectric inkjet nozzle, though it is generally suitable for capturing some remnant of static viscoelastic behaviour, if present, which should be avoided in respect of initiating ink ejection from the print head chamber. However, especially polymer solutions, such as the PS ink, may have different rheological behaviour under high shear rates due to thixotropic and shear-induced viscoelastic effects. Ink flow in confined regions through the print head, in respect of the combination of microscale channels in the head (typically 10–100 µm) and the associated volume flow rate(s), results in these high shear rate effects.

The jetted ink volumes and hydrophobising agent contents per unit area as a function of drop spacing are listed in Table 6 for both inks, calculated based on the measured drop mass. The values shown do not take into account the ink spreading taking place on the substrate, depending on the substrate properties, printing conditions and printed pattern.

3.3 Ring tests with PS ink and water

With PS ink, reliable hydrophobic ring test patterns were successfully printed on all tested binder-containing coatings, on condition that sufficient amount of ink was applied. Table 7 specifies the number of printed layers with different drop spacing settings required for reliable hydrophobic barriers on coatings with PS ink. The table also lists the weight (w/w) ratio of applied polystyrene to that of the porous layer (coating or filter paper), with the weight calculated from coating or filter paper basis weight and the actual area of the printed ring, as well as the volume (v/v) ratio of a single ink layer to that of the pore volume under the printed area, with the pore volume calculated based on the actual area of the printed ring, basis weight and combined specific pore volume.

The only case where no reliable hydrophobic ring could be produced was on the pure FCC105 coating, with no binder included. However, with this coating, using 10-µm drop spacing and 4 or 5 layers of PS ink came very close to producing ring barriers that worked, reporting success for 6 or 7 out of 8 tested rings, respectively. PS ink

Table 6 Jetted ink volume and hydrophobising agent contents per unit area, as a function of drop spacing

Ink	Ink volume per unit area (cm^{3}m^{-2})			Hydrophobising agent per unit area (g m^{-2})		
	10 µm	15 µm	20 µm	10 µm	15 µm	20 µm
PS	93.0 ± 12.8	41.3 ± 5.7	23.3 ± 3.2	4.0 ± 0.6	1.8 ± 0.2	1.0 ± 0.1
AKD	96.5 ± 7.0	42.9 ± 3.1	24.1 ± 1.7	4.2 ± 0.3	1.8 ± 0.1	1.0 ± 0.1

Values given with 95 % confidence intervals

Table 7 Number of printed layers required to produce effective ring barriers with PS ink at different drop spacing values

Substrate	Number of ink layers at drop spacing			PS to porous layer ratio (w/w)			Ink to pore volume ratio (v/v)		
	10 μm	15 μm	20 μm	10 μm	15 μm	20 μm	10 μm	15 μm	20 μm
GCC12 + MFC A	2 layers	2 layers	5 layers	0.20	0.06	0.13	22.66	7.83	5.89
FCC40 + MFC A	2 layers	4 layers	No barrier	0.31	0.26	–	12.48	5.13	–
FCC105 + MFC A	3 layers	No barrier	Not tested	0.96	–	–	6.99	–	–
FCC105 + MFC B	1 layer	2 layers	4 layers	0.78	0.60	0.86	6.44	2.49	1.76
FCC105 + MCC	3 layers	No barrier	Not tested	0.82	–	–	1.63	–	–
FCC105 + CMC	3 layers	No barrier	Not tested	0.75	–	–	1.97	–	–
FCC105 + PVOH	3 layers	No barrier	Not tested	0.70	–	–	2.74	–	–
FCC105 + latex	1 layer	1 layer	No barrier	0.35	0.14	–	2.86	1.21	–
FCC105 + sodium silicate	3 layers	No barrier	Not tested	0.64	–	–	2.37	–	–
FCC105	No barrier	No barrier	Not tested	–	–	–	–	–	–
Whatman 4	3 layers	No barrier	Not tested	0.15	–	–	0.94	–	–

"No barrier" indicates no reliable barrier was achieved with 5 printed layers

hydrophobises porous material by having polystyrene molecules adsorb onto pore surfaces and covering the native surface chemistry. The difficulty in hydrophobising the native FCC105 pigment, when comparing with the same pigment mixed with binders, might be due to the higher specific surface area of the native pigment requiring a greater amount of hydrophobic agent to cover it and/or the inability of the larger ink polymer molecules to enter the nanopore structure, which is accessible by water molecules, and observed by both the nitrogen adsorption used for measuring specific surface area and permeation under pressure in the mercury porosimetric evaluation.

As regards the coatings containing binder, it was possible with the 10-μm drop spacing to generate reliable barriers on all of them, though typically necessitating multiple printed ink layers. This drop spacing setting provided the highest tested ink volume per substrate area ratio. Interestingly, in this study, Whatman 4 filter paper required 3 layers for successful hydrophobisation, compared with an earlier study by the authors where a single layer with similar ink, albeit applying a different test pattern and different print settings, was sufficient (Koivunen et al. 2015). The difference in ink demand is likely to be due to smaller drop sizes related to different print settings, though unfortunately drop mass was not measured in the earlier study to support this supposition. While 3 layers were sufficient to hydrophobise the Whatman 4 in the present study, we see that this same loading was also sufficient to hydrophobise any of the binder-containing coatings. However, making such a comparison requires that the high basis weight of the filter paper should also be taken into consideration, i.e., a lower weight of polystyrene at 10-μm drop spacing was required to hydrophobise a unit weight of Whatman 4 than per unit weight of any of the coatings. To understand this

relationship is complex, since cellulose fibres are highly reactive to water, including dimensional change (swelling), fibre interstitial water absorption and fibril internal water sorption, returning a typical specific surface area for BET water sorption of ~128 m^2g^{-1}. However, the mechanism of hydrophobising is not only related to surface chemistry but is highly dependent on length scale. The length scale of cellulose fibres is far greater than that of pigments (frequently greater than ×10), and so it is possible on cellulose fibres to achieve hydrophobising via the well-known paper sizing mechanism, whereby only surface spots of hydrophobicity on a fibre are required to halt the wetting line for water as it travels the surface length of the fibre, i.e., not all the surface area requires to be hydrophobised in order for a fibre matrix filter paper to exhibit non-wetting by water. The pore structure of coatings, in contrast, inevitably requires hydrophobising minimally at the points of permeation pore connectivity, which are necessarily more numerous than the required points of hydrophobising along a fibre length due to the significantly shorter length scale of the coating structure.

With the 15-μm drop spacing, reliable barriers were produced on four of the different coatings. As little as a single ink layer was seen to be sufficient to hydrophobise the FCC105 + latex coating at this drop spacing. This effect is presumably due to the reduced pore connectivity and/or surface area caused by the binder, as well as the latex itself resulting in less hydrophilic pore surface chemistry.

At 20-μm drop spacing, reliable barriers with PS ink were produced only on the GCC12 + MFC A and FCC105 + MFC B coatings. This is presumably due to these two coatings being significantly thinner than the rest, enabling full-depth penetration of the coating with a lower applied ink volume. As for other substrates, most of them

were not even tested with this drop spacing, due to failing to produce reliable barriers already with the 15-µm drop spacing.

Examination of the ink to pore volume ratio v/v in Table 7 shows that ratios are almost always higher than 1, with the exception of Whatman 4, which is slightly below. Values above 1 indicate that the volume of the ink applied per layer is larger than the native pore volume that the print has actually covered. This is possible due to the relatively slow speed of the printer, allowing significant amounts of solvent to evaporate during the printing and freshly deposited ink to flow to previously printed regions that have already partially dried. With a high-speed printing set-up, such an effect would be significantly reduced, possibly replaced instead by higher pattern spreading due to excess ink flowing into empty pores, and poorer hydrophobisation due to lower concentration w/w of polystyrene to coating in the final paperfluidic device.

3.4 Ring tests with AKD ink and water

In the case of AKD ink, reliable barriers were produced on every tested coating except on the one employing sodium silicate as a binder. Table 8 lists the number of printed layers required to form reliable hydrophobic barriers on the various coating substrates with AKD ink. Ratio w/w or v/v of AKD to coating has not been calculated, due to difficulties in determining the exact treated area from the samples and due to most samples only requiring a single layer of AKD, thus lacking differentiation at the lower limit of ink volume applied.

Table 8 Number of printed layers required to produce effective ring barriers with AKD ink

Substrate	Number of ink layers at drop spacing		
	10 µm	15 µm	20 µm
GCC12 + MFC A	1 layer	1 layer	1 layer
FCC40 + MFC A	1 layer	1 layer	1 layer
FCC105 + MFC A	1 layer	2 layers	2 layers
FCC105 + MFC B	1 layer	1 layer	1 layer
FCC105 + MCC	1 layer	1 layer	2 layers
FCC105 + CMC	1 layer	1 layer	1 layer
FCC105 + PVOH	1 layer	1 layer	1 layer
FCC105 + latex	1 layer	1 layer	1 layer
FCC105 + sodium silicate	No barrier	No barrier	No barrier
FCC105	1 layer	1 layer	No barrier
FCC105 (not heated)	1 layer	2 layers	No barrier
Whatman 4	1 layer	1 layer	1 layer

"No barrier" indicates no reliable barrier was achieved with 2 printed layers. All samples were heat-treated post-printing, except for the one indicated as "(not heated)"

The hydrophobisation mechanism of AKD is based on reaction with hydroxyl groups. These groups can be found on FCC in the form of hydroxylapatite, as well as in cellulose and polyvinyl alcohol, but not on sodium silicate. Presumably, the large amounts of sodium silicate (50 parts w/w to 100 parts of FCC105) covered the hydroxylapatite surfaces on FCC105 + sodium silicate coating to such an extent that there was little or no native pigment surface left for the AKD to react with. However, increased amounts of deposited AKD still reduced the extent of spreading of drops on the coating, suggesting that even the unreacted AKD was able to reduce spreading on this coating.

For the binders other than sodium silicate, therefore, AKD ink provided effective hydrophobisation on all the tested drop spacing settings and with fewer ink layers than required for PS ink. Superior performance at 15- and 20-µm drop spacing values suggests that AKD ink, with lower viscosity, penetrates deeper into the substrate than PS ink. The lower number of layers required indicates that AKD is more effective in hydrophobising, possibly due to a smaller molecular size allowing it to spread more evenly or to occupy a greater number of key hydrophobising points. Furthermore, instead of only covering highly hydrophilic hydroxyl groups on the coating pore surface, it replaces them with hydrophobic hydrocarbon chains.

The aspect of hydrophobising agent positioning within the porous network structure is itself considered to be self-optimising in two ways, (1) the concentration of the hydrophobising agent will be greater where the greater volume of the liquid phase of the ink has flowed during its application, and, thus, is correctly positioned to prevent subsequent flow after treatment, and (2) assuming a mechanism of pore surface adsorption, as proposed here, will provide an optimal distribution of the AKD over the original hydrophilic sites driving the wetting force.

As with PS ink, pure FCC105 coating without binder proved to be slightly more difficult to hydrophobise than the same pigment combined with binder, with the pigment alone not reliably hydrophobised at 20-µm drop spacing. This coating was also tested without post-printing heat treatment, in which case reliable barriers could be produced, though requiring 2 layers instead of 1 at 15-µm drop spacing. As mentioned earlier, AKD was originally designed for hydrophobising cellulose fibres and for that application heat treatment is generally considered as a necessary step to ensure that AKD molecules react with hydroxyl groups. Most commercial paper coating pigments do not feature hydroxyl groups and thus are unlikely to react with AKD, with FCC forming an exception.

As an alternative to a solvent-based solution, AKD can be printed as aqueous emulsion (Wang et al. 2014), reducing solvent emissions from the printing process. With plain cellulosic paper, such an ink could be problematic for mass

production, since the water volumes involved might result in weakening of inter-fibre bonds while wet, possibly leading to web breaks in roll-to-toll production, and in curling of the paper while drying. However, with multi-layer coatings, as discussed in the introduction, the base paper can be isolated from the aqueous emulsion, thus avoiding runnability issues. The main drawback of aqueous AKD emulsion compared with xylene-based solution, as employed in this study, could be limited emulsion shelf life due to spontaneous reaction between AKD and water, as well as possible challenges in colouring it while developing water fastness in subsequent practical applications.

3.5 Ring tests with AKD ink and low surface tension liquids

In addition to dyed water, ring tests were performed also with low surface tension liquids, consisting of five ethanol solutions and one surfactant solution. These were tested on the ring test pattern printed on the MFC105 + MFC A coating with 2 layers of AKD ink applied at 20-μm drop spacing, found previously to be able to contain water in the same test environment. Properties of the test liquids and their performance in breaching the AKD ring are listed in Table 9. Minor leaking indicates that the liquid spreads beyond the inner boundary of the ring, while major leaking indicates that it spreads beyond the outer boundary of the ring.

Testing of hydrophobic printed barriers with low surface tension liquids has been performed previously both with aqueous surfactant solutions (Olkkonen et al. 2011) and with various organic solvents (Maejima et al. 2013; Wang et al. 2014). The test liquids in the present work are likely to undergo a dynamic surface tension shift during drying of the liquid drop. In case of surfactant solution, surface tension is expected to decrease during drying as surfactant concentration increases, while for water–ethanol solutions surface tension is expected to increase as ethanol presumably evaporates faster from the surface than water. The latter

Table 9 Properties of aqueous low surface tension liquids

Ethanol content (w/w%)	Surfactant content (w/w%)	Surface tension (mN m^{-1})	AKD ring penetration
0	1	45.2 ± 0.7	Major leaking
15	0	44.1 ± 0.8	Holds
20	0	39.3 ± 1.4	Holds
25	0	36.4 ± 1.0	Minor leaking
30	0	33.7 ± 0.9	Minor leaking
40	0	30.1 ± 0.4	Major leaking

Surface tension listed with 95 % confidence interval

phenomenon was experimentally confirmed for the test liquids with surface tension of drops monitored for 10 min during drying (data not included). Additionally, in the case of the surfactant solution, we may also expect Marangoni ("coffee stain") effects to occur, in which the surfactant concentration will increase even further at the interface between the test solution and the barrier, thus increasingly aiding wettability. Surface tension values given in Table 9 are for a fresh drop prior to any evaporation.

As shown in Table 9, increasing ethanol content in ethanol–water solutions resulted in decreased surface tension and increased containment ring penetration, with solutions up to 20 w/w% held fully within the ring. Initially unexpectedly, the surfactant solution, which had higher surface tension than the water–ethanol solutions, could penetrate the rings. However, this becomes less surprising when we consider the effects of surfactant differential concentration discussed previously. For comparison, in a previous study of printed AKD barriers on Whatman 1 filter paper, dimethyl sulfoxide (43 mN m^{-1}) and glycerol (64 mN m^{-1}) could be contained by the barriers, while the same barriers were penetrated by methanol (22 mN m^{-1}), isopropanol (23 mN m^{-1}), toluene (28 mN m^{-1}) and 1 % Triton X-100 solution (33 mN m^{-1}) (Wang et al. 2014).

After the low surface tension test liquids in the present evaluation had dried, fresh 10-μl drops of rhodamine B-dyed water were applied to the rings that had been penetrated by surfactant solution and 40 w/w% ethanol solution. When applied to the surfactant-penetrated ring, almost immediate major leaking of the water resulted, while on the ethanol-penetrated ring, only slow minor leaking resulted. This suggests that the surfactant had not only concentrated at the barrier interface but had adsorbed to the hydrophobised areas, turning them hydrophilic. Although ethanol solution would be expected not to have been able to affect reacted AKD, it may have transported unreacted AKD molecules with the flow, thus reducing the hydrophobicity of the ring barrier. This could explain why some subsequent penetration by post-added water could occur, though far less than in the case of the surfactant. The results suggest that surfactant solutions and organic solvents may penetrate hydrophobic barriers to different degrees and in different manners, and that results obtained for surfactant solution of a given surface tension may not necessarily apply to organic solvent solution of similar surface tension, and vice versa. The ability of the surfactants to convert hydrophobised pore surfaces back to hydrophilic can also be applied to create paperfluidic valve mechanisms (Chen et al. 2012).
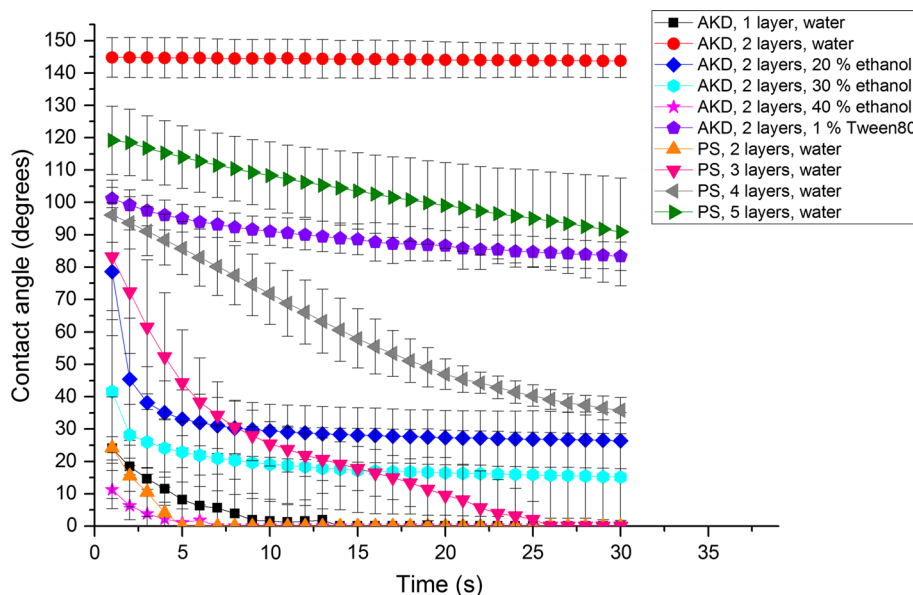
3.6 Surface contact angles

To evaluate further the interaction between water and low surface tension liquids with hydrophobised areas,

Fig. 6 Contact angle of liquid as a function of time for various printed surfaces on FCC105 + MFC A coating, with 95 % confidence intervals

10 × 170 mm² rectangles were printed on the same FCC105 + MFC A-coated PP substrate, as used for the previous experiments, with both PS and AKD inks. PS ink was printed at 15-μm drop spacing and 1–5 layers, while AKD ink was printed at 20-μm drop spacing and 1–2 layers. Contact angle as a function of time was measured for all of these printed surfaces, as well as unprinted coating, with deionised water. Surface printed with 2 layers of AKD ink was additionally measured with 20, 30 and 40 w/w% ethanol solutions and 1 w/w% Tween 80 surfactant solution. Measured liquid contact angles as a function of time are presented in Fig. 6.

In the case of either incompletely hydrophobised or unprinted surface, the understanding of what is meant by contact angle cannot follow classical models when the surface is completely hydrophilic. This is due to the presence of a connected network of pores acting 3-dimensionally beneath and at the limits of the drop meniscus, in which liquid may absorb and be transported both into the sample pore volume and laterally internally in the structure independent of the bulk contact meniscus. In turn, this transported liquid acts to distort the bulk contact meniscus should it be found to emanate from the surface beyond the limits of the droplet. In this case, one can only record an apparent contact angle since the pore structure cannot be considered as a surface roughness in a classical Wenzel case (Wenzel 1936). In the case of strongly hydrophobised coatings, a Cassie–Baxter droplet surface configuration (Cassie and Baxter 1944) could in theory, however, be assumed.

In the present study, reduction in measured contact angle for liquid as a function of time was largely due to reduction in measured drop volume caused by absorption of the drop into the coating. In the case of either unprinted coating or after 1 layer of PS ink is applied, this absorption was so fast that no apparent contact angle could be determined, and so these samples are omitted in Fig. 5 for clarity. For the other PS ink printed samples, the apparent contact angle increases as the number of printed layers increases, but always remains under 90° after 30 s. None of these PS ink print settings produced reliable barriers with the ring test, either.

With AKD ink, 1 layer results in a retained very low apparent contact angle with water, while 2 layers result in quite high contact angle of over 140°. With ethanol solutions, contact angles are under 90°, with increasing ethanol content resulting in further lowering of the contact angle. This also applies for 20 w/w% ethanol solution, which could not penetrate the ring test pattern, but on this test could, nonetheless, be observed to be absorbed into the coating. This suggests that there may be uneven distribution of AKD within the printed area, with higher concentrations on the print edges, which form the critical barrier region within the ring test pattern, and a reduced concentration in the central print areas where the drop is applied during the contact angle measurements. Such uneven distribution of AKD from solution likely results from Marangoni flows, i.e., the oft-observed coffee stain effect, also discussed previously in the case of surfactant concentration distribution, transporting AKD to the edges of the printed pattern during drying. With Tween 80 solution, the contact angle is initially above 90°, but goes progressively below 90° within 30 s. This is related to the typical diffusion delay before surfactant can concentrate sufficiently at the wetting front.
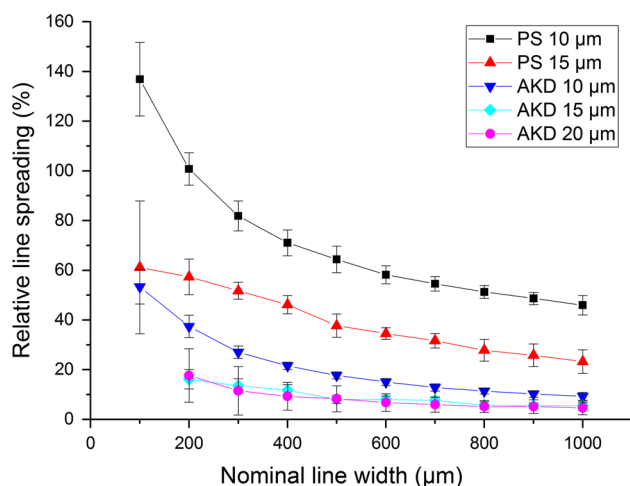
Fig. 7 Relative line widths for various printed lines on FCC105 + MFC A coating, expressed as percentage gain in relation to nominal line width
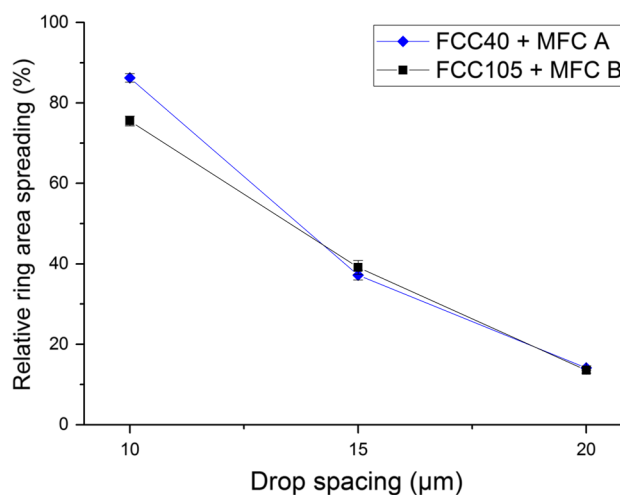

Fig. 8 Relative ring area spreading as a function of drop spacing for rings printed with PS ink on FCC40 + MFC A and FCC105 + MFC B coatings

3.7 Line and ring spreading

Line spreading as a function of nominal line width was evaluated for a few selected combinations of ink and print settings on the MFC105 + MFC A coating, applying the line spreading test pattern. With both PS and AKD inks, only a single layer of ink was printed for this pattern. Figure 7 displays the measured line widths, where the values shown are measured from the colourant contained within the inks, and not from the actual hydrophobising agent, since the latter cannot be optically identified by a scanner. It is possible that the hydrophobising agent has in some cases spread farther than the colourant. AKD ink samples were printed with added blue dye colourant, producing sharply defined patterns. Line spreading was measured from 3 samples in the case of PS inks and from 9 samples for AKD containing inks.

As shown in Fig. 7, narrower lines spread relatively more than wider lines. Assuming that the hydrophobising agent would spread evenly over this area, this would then result in fine patterns having a lower concentration of said agent per unit area. However, as we saw earlier due to the edge concentration effects, such even distributions of hydrophobising agent over the area may not actually occur. With PS ink, increasing the amount of ink volume per unit surface area, by reducing drop spacing from 15 to 10 μm, resulted in a noticeable increase in line spreading. For the AKD inks, the measured line spreading is lower than for the PS inks; this may be due to greater separation of the blue dye from the carrier solvent when compared with Sudan Red G.

Pattern spreading for the printed rings was also measured as a function of drop spacing, as shown in Fig. 8, for rings printed with PS ink on the two exemplified coatings.

The scanned rings have been printed with 3 (10-μm drop spacing) or 4 (15- and 20-μm drop spacing) layers of ink. In this case, the spreading is expressed in terms of relative increase in the ring area, i.e., two-dimensional gain rather than the one-dimensional gain measured for lines.

As shown in Fig. 8, increasing the applied ink volume to unit surface area ratio by reducing the drop spacing results in increased pattern spreading, though it also results in fewer layers required for hydrophobisation, as demonstrated previously in Table 7. Thus, applying higher volumes of PS ink to reduce the number of printed layers will also result in poorer resolution due to increased pattern spreading. Interestingly, the area spreading is very similar in both of the coatings, even though FCC105 + MFC B coating is significantly thinner. Furthermore, reducing the drop spacing resulted in the edges of the printed rings becoming more irregular. This can be expressed in terms of circularity, which is defined as

$$\text{Circularity} = 4\pi A P^{-2} \tag{1}$$

where P in this case is the exterior perimeter of the ring and A the area inside this perimeter. Circularity ranges from 0 to 1, with an ideal circle having the value 1 and lowering values expressing increasing deviation from the ideal. Evaluating with ImageJ software, the circularity of the rings printed with PS ink on FCC105 + MFC B, resulted in circularity values of 0.88 ± 0.02, 0.86 ± 0.03 and 0.65 ± 0.04 for the rings printed at 20-, 15- and 10-μm drop spacing, respectively.

3.8 Minimum channel width

Minimum channel width was evaluated with samples printed on FCC105 + MFC A coating with 2 layers of

AKD ink at 20-µm drop spacing. All tested channels allowed water to wick the full length of the channel within the observed 10 min time period. The narrowest channel measured as 468 ± 12 µm wide for a nominal width of 500 µm, with measurement once again taken from the scanned image defined by the colourant contained within the hydrophobic ink. For comparison, channels of 561 ± 45 µm width have been reported by the Whitesides group for chromatography paper patterned with a commercial hot melt wax inkjet printer (Carrilho et al. 2009a), while channels of 272 ± 19 µm width have been achieved with experimental inkjet printed UV-curing polymer on filter paper (Maejima et al. 2013).

Even narrower channels than the ones tested in this study are likely to be achievable with custom-designed pigment coatings by applying thinner coatings and more carefully selected ink volumes than considered in this study. Furthermore, the laboratory rod coating method used in this study is likely to limit the achievable channel resolution, since it tends to produce local variation in coating thickness, which can result in uneven printed pattern edge definition as lateral ink spreading differs between thinner and thicker regions of coating. The extent of local variation in coating thickness was not explicitly studied in this work. Other coating methods, such as standard blade and smooth bar rod coating, would be expected to produce more even results, with the most preferable likely to be curtain coating for the application of these speciality porous structured coatings.

Channel and barrier dimensions together define how many parallel assays can fit within a given substrate area. For self-contained assays to be used in the field, the capabilities of the unaided eye as assessor of the result(s) set their limitations for device design, since colorimetric devices with very small detection zones may become difficult to read. However, for platforms intended to be used as research tools in laboratories, where external readers and microscopes are readily available, fine resolution may allow for larger numbers of assays to be run on parallel, thus increasing efficiency.

The wicking front travel times for individual channels were not measured in this study, but water seemed to travel quicker on the wider channels than on the narrower channels. This observation matches with previous studies of printed wax channels on cellulose filter papers, on which water was discovered to travel slower in narrower printed channels (Hong and Kim 2015). This is likely to be related to the constriction effects of the narrower channels involving the barrier edge non-uniformity and dependence on viscous flow in restricted capillary regions.

3.9 Minimum barrier width

Minimum barrier width was evaluated with sample prints on FCC105 + MFC A coating with 2 layers of AKD ink at 20-µm drop spacing. The narrowest achievable reliable barrier had, coincidentally, also 500 µm nominal width and was measured as 496 ± 12 µm real width, based on colourant. For comparison, in a previous study by the authors, barriers of 566 ± 191 µm could be patterned on Whatman 4 filter paper using 6 w/w% AKD ink without colourant (Koivunen et al. 2015), while barriers of 850 ± 50 µm width have been reported for chromatography paper with wax printing (Carrilho et al. 2009a) and barriers of 425 ± 26 µm width have been reported for UV-curing polymer on filter paper (Maejima et al. 2013). As with channels, narrower reliable barriers on coatings may be achievable by thinner coating layers.

Close observation of the barrier test samples after testing revealed slight spreading of test liquid that had breached a barrier into the walls separating the channels beyond the barrier. This phenomenon is illustrated in Fig. 9. Of particular interest is that this spreading does not seem to happen evenly, as can be seen from the detail shown in Fig. 9b. No such phenomenon could be observed on ring test patterns with the same coating and print settings.

3.10 Effect of printing on coating pore structure

A study was conducted to test the feasibility of measuring the effect of printed hydrophobising on the coating pore structure. For this, 30×130 mm^2 rectangles were printed on FCC40 + MFC A and FCC105 + MFC A coatings, applied on aluminium foil, with various print settings. Chosen coatings, print settings and resulting specific pore volumes, with cut-off diameters as previously defined, are listed in Table 10. Samples printed with AKD ink, coloured with yellow dye, were tested both with regular post-printing heat treatment ("heat-treated") and without heat treatment ("no heating") in order to investigate whether the heating would affect spreading.

Due to the exploratory nature of this part of the study, only a single sample was measured per print setting. However, the results seem to indicate that changes in pore volume resulting from the deposition of the printed hydrophobic agent can be detected with this method. Thus, the method can be applied in future with larger sample sizes to evaluate statistical significance of the measured changes. The results also demonstrate that only part of the pore volume is filled by the hydrophobising agent, as could be expected to take place with inks of only 5 w/w % dry solid content. This again confirms that the blocking of capillary transport within the pores is by surface chemistry modification, not by the filling of pores. Regarding the blocking of liquid spreading, only one of the settings used for PS ink, that of 5 layers on FCC40 + MFC A, could actually produce reliable barriers with the ring test pattern. AKD ink on the other hand was deposited with settings that would produce reliable barriers with the ring test, at least if heat-treated post-printing.

Fig. 9 Spreading of test liquid after breaching the barrier: **a** scanned picture of channels and walls beyond breached barriers, **b** optical microscope picture showing detail of one inter-channel wall
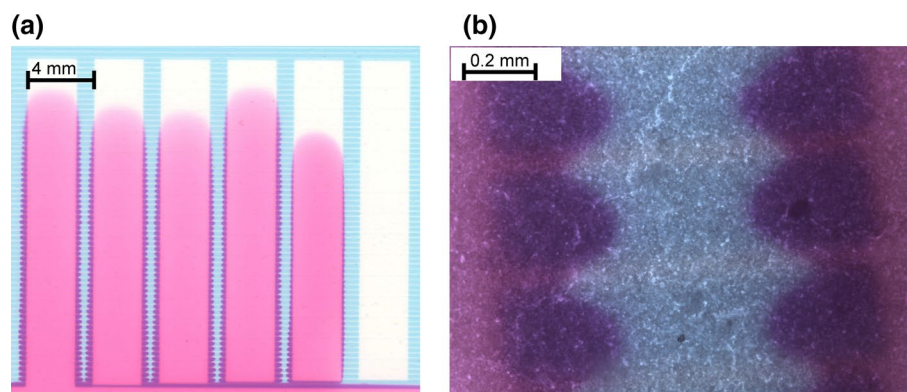

Table 10 Specific pore volume as a function of printed layers

Coating	Printed ink	Intra-particle specific pore volume ($cm^3 g^{-1}$)	Inter-particle specific pore volume ($cm^3 g^{-1}$)	Combined specific pore volume ($cm^3 g^{-1}$)	$d*$ (μm)	$d**$ (μm)
FCC40 + MFC A	None	0.12	0.18	0.30	0.18	1.8
FCC40 + MFC A	AKD, 2 layers, no heating	0.12	0.18	0.30	0.18	1.8
FCC40 + MFC A	AKD, 2 layers, heat-treated	0.13	0.20	0.33	0.18	1.8
FCC40 + MFC A	PS, 1 layer	0.11	0.18	0.29	0.18	1.8
FCC40 + MFC A	PS, 2 layers	0.08	0.18	0.26	0.18	1.8
FCC40 + MFC A	PS, 5 layers	0.02	0.14	0.16	0.18	1.8
FCC105 + MFC A	None	0.46	0.59	1.05	0.64	7.8
FCC105 + MFC A	AKD, 2 layers, no heating	0.36	0.46	0.82	0.64	7.8
FCC105 + MFC A	AKD, 2 layers, heat-treated	0.37	0.53	0.90	0.64	7.8
FCC105 + MFC A	PS, 1 layer	0.42	0.58	1.00	0.64	7.8
FCC105 + MFC A	PS, 2 layers	0.35	0.51	0.86	0.64	7.8
FCC105 + MFC A	PS, 5 layers	0.29	0.51	0.80	0.64	7.8

AKD ink printed with 20-μm drop spacing, PS ink printed with 15-μm drop spacing

4 Conclusions and future work

This study demonstrates the feasibility of printing hydrophobic patterning on coatings consisting of hydrophilic, nanoporous FCC and a variety of binders. However, such coatings are challenging to hydrophobise, as demonstrated by the numerous cases where printing of multiple ink layers was required for reliable local hydrophobisation of the coating. Compared with cellulose filter papers, a higher amount of hydrophobising agent was required to hydrophobise a unit weight of porous material. This may be due to the much shorter length scale of the coating compared with ordinary cellulose fibres and the highly hydrophilic nature of the pigment contained in the coatings. Even lower surface area GCC12 + MFC A coating required multiple layers of polystyrene ink for reliable barriers, supporting the relation to shorter length scale and resulting greater complexity of the coating pore network.

Although the speciality pigment FCC features a highly hydrophilic surface chemistry and highly porous structure, it does not solely dominate the wicking nature of the coating. This becomes apparent when comparing the wicking speeds for the different coatings, which varied significantly based on the chosen binder. Also, different versions of FCC result in different wicking speeds, as can be seen from comparison of FCC40 + MFC A and FCC105 + MFC A coatings, where FCC105-containing coatings demonstrate clearly superior wicking speeds related predominantly to the higher surface area and associated greater pore number. In future, the authors will also test coatings featuring an FCC version with higher specific surface area than those presented in this study, and this is expected to result in faster wicking speeds.

The high specific surface area of FCC pigments can provide unique advantages for diagnostic applications. For example, if the substrate is used for chromatographic separation of sample liquids, solutes and/or suspended colloidal

particles, either by virtue of the native FCC surface chemistry or by further surface treatment, there is a larger surface area for sample to adsorb on or otherwise interact with. Finally, the volume capillary wicking capacity control of speciality coating structures including FCC clearly offers an advantage over that of traditionally applied cellulosic filter paper.

FCC pigments presented in this study are experimental and not commercially available. Thus, at the time of the writing, it is not possible to give a reliable cost comparison estimate for the presented materials and coatings when produced on the industrial scale. For practical applications, the coating also requires a barrier-coated paper as a base substrate for mechanical support, though relatively inexpensive base paper and commercial coating materials can be utilised for this.

Regarding the inks tested in this study, alkyl ketene dimer (AKD) provides a clearly superior performance in hydrophobising compared with polystyrene (PS). The drawbacks of the tested AKD ink process-wise are the required low jetting frequency, resulting from low viscosity, and the assumed need for heat treatment. However, jetting frequency can in principle be increased with rheological modifiers, while the results of this study showed that heat treatment might not always be imperative, as demonstrated when used with pure FCC105 coating. The possible synergistic reactions taking place between FCC and AKD were not studied in sufficient detail to provide absolute confirmation of their efficacy. An additional advantage of AKD ink is that the dry solids content can be further increased to reduce the need to deposit 2 successive layers when printing, as was required by some of the tested coatings.

Compared with AKD ink, which mostly required only a single ink layer, PS ink generally required multiple printed layers to produce reliable barriers. While this can be interesting for research purposes, it tends to be undesirable from a manufacturing point of view, especially since the previous ink layer needs to sufficiently dry before a new one is deposited. Furthermore, increasing the dry solids content of the PS ink would require a polystyrene version with even lower molecular weight than the 35 kDa in this study. However, the advantage of PS ink is that it does not require post-print treatment.

From a pragmatic point of view, hydrophobising of FCC-containing coatings could be improved by either a further alternative hydrophobising agent or ink formulation, which would be able to produce reliable barriers with a single printed layer but would not require a separate heating or other post-processing step after drying. Phase-changing inks, jetted as liquids but then solidified by cooling (hot melt), polymerisation or cross-linking would allow for significantly higher hydrophobic material content in the ink than any solvent-based ink, though they require an additional post-processing step, as well as sufficient time to permeate the pore network structure. Especially for research purposes, a hydrophobising agent with visible colour could be desirable, thus removing the need to add separate colourant for locating the printed regions, especially since some colourants may be able to act as partial surfactants.

Compared to Whatman 4 filter paper, the tested coatings demonstrated slower wicking speeds and required higher amounts of hydrophobising agent, making them inferior in these aspects. In order to improve performance, the coating materials, formulations and thicknesses need to be optimised. However, the performance of faster wicking coatings, especially those with MFC binders, can already be considered adequate for use as test substrates in prototype applications.

In future work, the authors intend to explore further variants of the coatings presented in this study, as well as more complex hydrophobic patterns that can be employed for practical applications. Selective surface modification of coatings will be tested to take advantage of their high surface area. Most importantly, the authors intend to demonstrate practical analytical applications with hydrophobically patterned pigment coating as base substrate. To this end, compatibility of the coatings and inks with various reagents, bioagents and detection methods will be studied, and the performance of custom coatings of various designs and thicknesses compared to conventional cellulosic filter papers.

Compliance with ethical standards

Conflict of interest The authors declare that they have no conflict of interest.

References

Apilux A, Ukita Y, Chikae M, Chailapakul O, Takamura Y (2013) Development of automated paper-based devices for sequential multistep sandwich enzyme-linked immunosorbent assays using inkjet printing. Lab Chip 13:126–135. doi:10.1039/c2lc40690j

Böhm A, Carstens F, Trieb C, Schabel S, Biesalski M (2014) Engineering microfluidic papers: effect of fiber source and paper sheet properties on capillary-driven flow. Microfluid Nanofluid 16:789–799. doi:10.1007/s10404-013-1324-4

Bollström R, Nyqvist R, Preston J, Salminen P, Toivakka M (2013) Barrier properties created by dispersion coating. Tappi J 12:45–51

Brunauer S, Emmett PH, Teller E (1938) Adsorption of gases in multimolecular layers. J Am Chem Soc 60:309–319. doi:10.1021/ja01269a023

Carrilho E, Martinez AW, Whitesides GM (2009a) Understanding wax printing: a simple micropatterning process for paper-based microfluidics. Anal Chem 81:7091–7096. doi:10.1021/ac901071p

Carrilho E, Phillips ST, Vella SJ, Martinez AW, Whitesides GM (2009b) Paper microzone plates. Anal Chem 81:5990–5998. doi:10.1021/ac900847g

Cassano CL, Fan ZH (2013) Laminated paper-based analytical devices (LPAD): fabrication, characterisation, and assays. Microfluid Nanofluid 15:173–181. doi:10.1007/s10404-013-1140-x

Cassie ABD, Baxter S (1944) Wettability of porous surfaces. Trans Faraday Soc 40:546–551. doi:10.1039/TF9444000546

Chen H, Cogswell J, Anagnostopoulos C, Faghri M (2012) A fluidic diode, valves, and a sequential-loading circuit fabricated on layered paper. Lab Chip 12:2909–2913. doi:10.1039/c2lc20970e

Chen Y, Kuo Z, Cheng C (2015) Paper—a potential platform in pharmaceutical development. Trends Biotechnol 33:4–9. doi:10.1016/j.tibtech.2014.11.004

Delaney JL, Hogan CF, Tian J, Shen W (2011) electrogenerated chemiluminescence detection in paper-based microfluidic sensors. Anal Chem 83:1300–1306. doi:10.1021/ac102392t

Di Risio S, Yan N (2010) Adsorption and inactivation behavior of horseradish peroxidase on various substrates. Colloid Surf B 79:397–402. doi:10.1016/j.colsurfb.2010.05.004

Evans E, Gabriel EFM, Coltro WKT, Garcia CD (2014) Rational selection of substrates to improve color intensity and uniformity on microfluidic paper-based analytical devices. Analyst 139:2127–2132. doi:10.1039/c4an00230j

Feng L, Li H, Niu L-Y, Guan Y, Duan C, Guan Y-F, Tung C, Yang Q (2013) A fluorometric paper-based sensor array for the discrimination of heavy-metal ions. Talanta 108:103–108. doi:10.1016/j.talanta.2013.02.073

Fenton EM, Mascarenas MR, Lopez GP, Sibbett SS (2009) Multiplex lateral-flow test strips fabricated by two-dimensional shaping. ACS Appl Mater Interfaces 1:124–129. doi:10.1021/am800043z

Hong S, Kim W (2015) Dynamics of water imbibition through paper channels with wax boundaries. Microfluid Nanofluid 19:845–853. doi:10.1007/s10404-015-1611-3

Hossain SMZ, Luckham RE, Smith AM, Lebert JM, Davies LM, Pelton RH, Filipe CDM, Brennan JD (2009) Development of a bioactive paper sensor for detection of neurotoxins using piezoelectric inkjet printing of sol − gel-derived bioinks. Anal Chem 81:5474–5483. doi:10.1021/ac900660p

Hossain SMZ, Ozimok C, Sicard C, Aguirre SD, Ali MM, Li Y, Brennan JD (2012) Multiplexed paper test strip for quantitative bacterial detection. Anal Bioanal Chem 403:1567–1576. doi:10.1007/s00216-012-5975-x

Jayawardane BM, McKelvie ID, Kolev SD (2012) A paper-based device for measurement of reactive phosphate in water. Talanta 100:454–460. doi:10.1016/j.talanta.2012.08.021

Jokerst JC, Adkins JA, Bisha B, Mentele MM, Goodridge LD, Henry CS (2012) Development of a paper-based analytical device for colorimetric detection of select foodborne pathogens. Anal Chem 84:2900–2907. doi:10.1021/ac203466y

Jutila E, Koivunen R, Gane PAC (2015) Effect of coating pigment, binder type and binder amount on planar wicking on coated substrates. J Print Media Technol Res 4:173–186. doi:10.14622/JPMTR-1419

Kim H, Noh H (2013) Quantifying the fluid volumes in paper microfluidic devices for dry eye test. Macromol Res 21:788–792. doi:10.1007/s13233-013-1081-y

Klasner SA, Price AK, Hoeman KW, Wilson RS, Bell KJ, Culbertson CT (2010) Paper-based microfluidic devices for analysis of clinically relevant analytes present in urine and saliva. Anal Bioanal Chem 397:1821–1829. doi:10.1007/s00216-010-3718-4

Koivula H, Pelton R, Brennan JD, Grenon J, Manfred T (2013) Flexographic printability of sol-gel precursor dispersions for bioactive paper. Nord Pulp Paper Res 28:450–457. doi:10.3183/NPPRJ-2013-28-03-p450-457

Koivunen R, Jutila E, Gane PAC (2015) Inkjet printed hydrophobic microfluidic channelling on porous substrates. J Print Media Technol Res 4:7–18. doi:10.14622/JPMTR-1413

Lamminmäki T, Kettle JP, Puukko P, Gane PAC, Ridgway C (2009) Inkjet print quality: the role of polyvinyl alcohol in speciality $CaCO_3$ coatings. J Pulp Pap Sci 35:137–147

Li X, Tian J, Garnier G, Shen W (2010) Fabrication of paper-based microfluidic sensors by printing. Colloid Surf B. 76:564–570. doi:10.1016/j.colsurfb.2009.12.023

Li C, Zhang H, Wu P, Gong Z, Xu G, Cai C (2011) Electrochemical detection of extracellular hydrogen peroxide released from RAW 264.7 murine macrophage cells based on horseradish peroxidase–hydroxyapatite nanohybrids. Analyst 136:1116–1123. doi:10.1039/c0an00825g

Li M, Junfei T, Al-Tamimi M, Shen W (2012) Paper-based blood typing device that reports patient's blood type "in writing". Angew Chem Int Ed 51:5497–5501. doi:10.1002/anie.201201822

Lu L, Zhang L, Zhang X, Huan S, Shen G, Yu R (2010a) A novel tyrosinase biosensor based on hydroxyapatite–chitosan nanocomposite for the detection of phenolic compounds. Anal Chim Acta 665:146–151. doi:10.1016/j.aca.2010.03.033

Lu Y, Shi W, Qin J, Lin B (2010b) Fabrication and characterization of paper-based microfluidics prepared in nitrocellulose membrane by wax printing. Anal Chem 82:329–335. doi:10.1021/ac9020193

Määttänen A, Fors D, Wang S, Valtakari D, Ihalainen P, Peltonen J (2011) Paper-based planar reaction arrays for printed diagnostics. Sens Actuator B-Chem 160:1404–1412. doi:10.1016/j.snb.2011.09.086

Määttänen A, Vanamo U, Ihalainen P, Pulkkinen P, Tenhu H, Bobacka J, Peltonen J (2013) A low-cost paper-based inkjet-printed platform for electrochemical analyses. Sens Actuator 177:153–162. doi:10.1016/j.snb.2012.10.113

Maejima K, Tomikawa S, Suzuki K, Citterio D (2013) Inkjet printing: an integrated and green chemical approach to microfluidic paper-based analytical devices. RSC Adv 3:9258–9263. doi:10.1039/c3ra40828k

Martinez AW, Butte MJ, Whitesides GM, Phillips ST (2007) patterned paper as platform for inexpensive, low-volume, portable bioassays. Angew Chem Int Ed 46:1318–1320. doi:10.1002/anie.200603817

Olkkonen J, Lehtinen K, Erho T (2011) Flexographically printed fluidic structures in paper. Anal Chem 82:10246–10250. doi:10.1021/ac1027066

Pelton R (2009) Bioactive paper provides a low-cost platform for diagnostics. TrAc-Trends Anal Chem 28:925–942. doi:10.1016/j.trac.2009.05.005

Ribeiro CC, Barrias CC, Barbosa MA (2004) Calcium phosphate-alginate microspheres as enzyme delivery matrices. Biomaterials 25:4363–4373. doi:10.1016/j.biomaterials.2003.11.028

Sameenoi Y, Nongkai PN, Nouanthavong S, Henry CS, Napapricha D (2014) One-step polymer screen-printing for microfluidic paper-based analytical device (μPAD) fabrication. Analyst 139:6580–6588. doi:10.1039/c4an01624f

Taudte RV, Beavis A, Wilson-Wilde L, Roux C, Doble P, Blanes L (2013) A portable explosive detector based on fluorescence quenching of pyrene deposited on coloured wax-printed micro-PADs. Lab Chip 13:4164–4172. doi:10.1039/c3lc50609f

Wang J, Monton MRN, Zhang X, Filipe CDM, Pelton R, Brennan JD (2014) Hydrophobic sol–gel channel patterning strategies for paper-based microfluidics. Lab Chip 14:691–695. doi:10.1039/c3lc51313k

Wenzel RN (1936) Resistance of solid surfaces to wetting by water. Ind Eng Chem 28:988–994. doi:10.1021/ie50320a024

Yang L, Wei W, Gao X, Xia J, Tao H (2005) A new antibody immobilization strategy based on electrodeposition of nanometer-sized hydroxyapatite for label-free capacitive immunosensor. Talanta 68:40–46

Yang X, Kanter J, Piety NZ, Benton MS, Vignes SM, Shevkoplyas SS (2013) A simple, rapid, low-cost diagnostic test for sickle cell disease. Lab Chip 13:1464–1467. doi:10.1039/c3lc41302k

Yetisen AK, Akram MS, Lowe CR (2013) Paper-based microfluidic point-of-care diagnostic devices. Lab Chip 13:2210–2251. doi:10.1039/c3lc50169h

Zhang Q, Chen C, Xie Q, Liu P (2009) Electrodeposition of a biocompatible hydroxyapatite matrix to immobilize glucose oxidase for sensitive glucose biosensing. Microchim Acta 165:223–229. doi:10.1007/s00604-008-0124-0

Zhao Z, Tian J, Wu Z, Liu J, Zhao D, Shen W, He L (2013) Enhancing enzymatic stability of bioactive papers by implanting enzyme-immobilized mesoporous silica nanorods into paper. J Mater Chem B 1:4719–4722. doi:10.1039/c3tb20953a

Zhong ZW, Wang ZP, Huang GXD (2012) Investigation of wax and paper materials for the fabrication of paper-based microfluidic devices. Microsyst Technol 18:649–659. doi:10.1007/s00542-012-1469-1